







Cite this: *RSC Adv.*, 2024, 14, 39381

Synthesis of novel pyridine and pyrazolyl pyridine conjugates with potent cytotoxicity against HepG2 cancer cells as PIM-1 kinase inhibitors and caspase activators†

Mohamed S. Nafie, ^{*ab} Ahmed Hamza,^{bc} Ahmed H. Moustafa, ^{*d} Hassan A. El-Sayed, ^{*de} Samir M. El Rayes, ^b Hesham A. Morsy^f and Ahmed Aboelmagd ^b

A novel series of nicotinonitrile and pyrazolyl nicotinonitrile were synthesized, and their PIM-1 kinase inhibitors and caspase activators were investigated. New Manich bases **6–8** were synthesized *via* reaction of pyridine **4** with piperidine, dimethyl amine, and morpholine in the presence of formalin. On the other hand, the pyrazolyl analogues **10–12** were synthesized *via* heterocyclization of acetohydrazide derivative **9** with acetylacetone, malononitrile, and ethyl cyanoacetate, respectively, in ethanol. The cytotoxic activity of compound **9** against MCF-7 and HepG2 cells was particularly noteworthy, with IC₅₀ values of 0.34 μ M and 0.18 μ M, respectively, among these derivatives. Compared to staurosporine with potent PIM-1 kinase inhibition, which had an IC₅₀ value of 16.7 nM and an inhibition of 95.6%, compound **9** had a strong inhibitory effect, with IC₅₀ values of 20.4 nM and 93.8%. It induced apoptosis activity in HepG2 cancer cells. Accordingly, compound **9** was proven to be an effective chemotherapeutic drug that targets PIM-1 in treating liver cancer.

Received 8th November 2024

Accepted 6th December 2024

DOI: 10.1039/d4ra07963a

rsc.li/rsc-advances

1 Introduction

Cancer is a dreadful disease that causes significant mortality worldwide. According to rough estimates, in 2024, 2 001 140 new cancer cases and 611 720 cancer deaths are projected to occur in the United States. Liver cancer, one of the leading causes of cancer-related deaths, has around 34 000 mortalities in the year 2024, and the numbers are still increasing.¹

PIM-1, a member of the calcium/calmodulin-dependent kinase (CaMK) family, is a serine/threonine kinase with a unique α C-helix-in/ α C-helix-out equilibrium and a catalytic domain structure that includes an activation loop, a C-terminal extension, and a P+1-loop. One of three isoforms (PIM1-3) was

first seen after retrovirus gene transformation; the most researched isoform is PIM-1.² The 44 kDa cytosolic protein encoded by PIM-1 is known to serve many roles in various solid and hematological malignancies that exhibit elevated enzyme expression. Moreover, PIM-1 phosphorylates integrin-linked kinase (ILK), which subsequently plays a role in invading human osteosarcoma cells. Additionally, PIM-1 kinase reduces ROS production in hepatocellular cancer and may be an important target for starting cytotoxicity.³

Many biological processes rely on PIM kinases, including apoptosis, cell proliferation, differentiation, and signaling pathways linked to cancer.⁴ Multiple studies have linked high PIM expression levels to human hematologic and epithelial malignancies, making these genes attractive therapeutic targets.⁵ The unique active location of PIM-1 kinase makes it easier to design tiny molecules that block the enzyme.⁶ Evidence shows that increases in PIM-1 are associated with carcinogenesis and metastasis.⁷ Several tumor types, including pancreatic, breast, prostate, hepatic, and colon cancers, showed elevated expression of PIM-1 kinase.⁸ This suggests that targeting PIM-1 with small-molecule medicines could be an effective way to halt cancer progression.⁹ Liver cancer is among the leading causes of cancer mortality, emphasizing the need for novel therapeutic agents. PIM-1 kinase, known for its role in apoptosis and cell survival, has emerged as a promising target due to its over-expression in hepatic malignancies. Pyridine and pyrazolyl

^aDepartment of Chemistry, College of Sciences, University of Sharjah, P.O. 27272, Sharjah, United Arab Emirates. E-mail: mohamed.elsayed@sharjah.ac.ae

^bDepartment of Chemistry, Faculty of Science, Suez Canal University, Ismailia, 41522, Egypt. E-mail: mohamed_nafie@science.suez.edu.eg

^cDepartment of Community Health, Community Health, Diwaniyah Technical Institute, Al-Furat Al-Awsat Technical University, Kufa, Iraq

^dDepartment of Chemistry, Faculty of Science, Zagazig University, Zagazig, 44519, Egypt. E-mail: hasanneg@gmail.com; ah_hu_mostafa@yahoo.com

^eAlzahravi University College, Karbala, Iraq

^fHigher Institution of Engineering & Modern Technology, El Marg, Cairo, Egypt

† Electronic supplementary information (ESI) available: Spectroscopic characterizations of the synthesized compounds are provided as ESI. See DOI: <https://doi.org/10.1039/d4ra07963a>



derivatives, widely recognized for their biological versatility, offer an excellent platform for developing kinase inhibitors.

The heterocyclic molecules are highly valued in drug design and development due to their natural origin and the presence of a versatile pharmacophore that exhibits biological activity. Notably, approximately 90% of bioactive pharmaceuticals contain a heterocyclic moiety,¹⁰ and over 75% of FDA-approved marketed drugs feature a heterocyclic analog with nitrogen in their ring structure^{11–13} Pyridine is a vital class of compounds characterized by a six-membered ring structure containing one nitrogen atom. Pyridine derivatives are the most common and significant heterocyclic compounds, which show their fundamental characteristics to various pharmaceutical agents and natural products.^{14,15} It also serves as an important structural unit in numerous pharmaceuticals,^{16,17} and the pyridine moiety is associated with a wide range of biological activities, including anti-cancer, antiviral, analgesic, and antioxidant properties.^{8–10} Interestingly, pyridine-based structures (**V–VIII**), including nicotinonitrile were able to induce PIM-1 kinase inhibition and exhibited promising anti-cancer activities (Fig. 1).^{18–20} Pyrazole-based structures (**I–IV**), belonging to the class of azoles, are highly effective heterocycles that play a crucial role in drug chemistry, as well as in biological and photochemical

properties. Moreover, the pyrazole scaffold is highly versatile and is utilized in a wide range of drugs that exhibit a broad spectrum of pharmacological activities, including anti-infective anti-cancer through PIM-1 kinase inhibition (Fig. 1).^{25,26} As seen in Fig. 1B with molecular visualization of PIM-1 kinase protein of the co-crystallized ligand making analyses of lipophilic and hydrophobic moieties to highlight the importance of cyanopyridine-based compounds.

Apoptosis and cell cycle progression are two of the most important biological processes, and PIM kinases play an essential role in regulating these proteins. Notably, Pim kinases are overexpressed in liver cancer. Therefore, they are seen as promising targets for the development of new therapies that target the liver.^{4,27}

One useful method in medicinal chemistry is the Mannich reaction, which is used to synthesize novel chemical compounds with important biological features. Pharmacological activity, bioavailability, and effectiveness are all affected by the physicochemical properties of prospective drug candidates, which can be altered using this process. Pharmaceutics and medicinal chemistry are persistently interested in Mannich bases because of their helpful biological activities and techniques of synthesis.²⁸ Given all this, the pharmacological

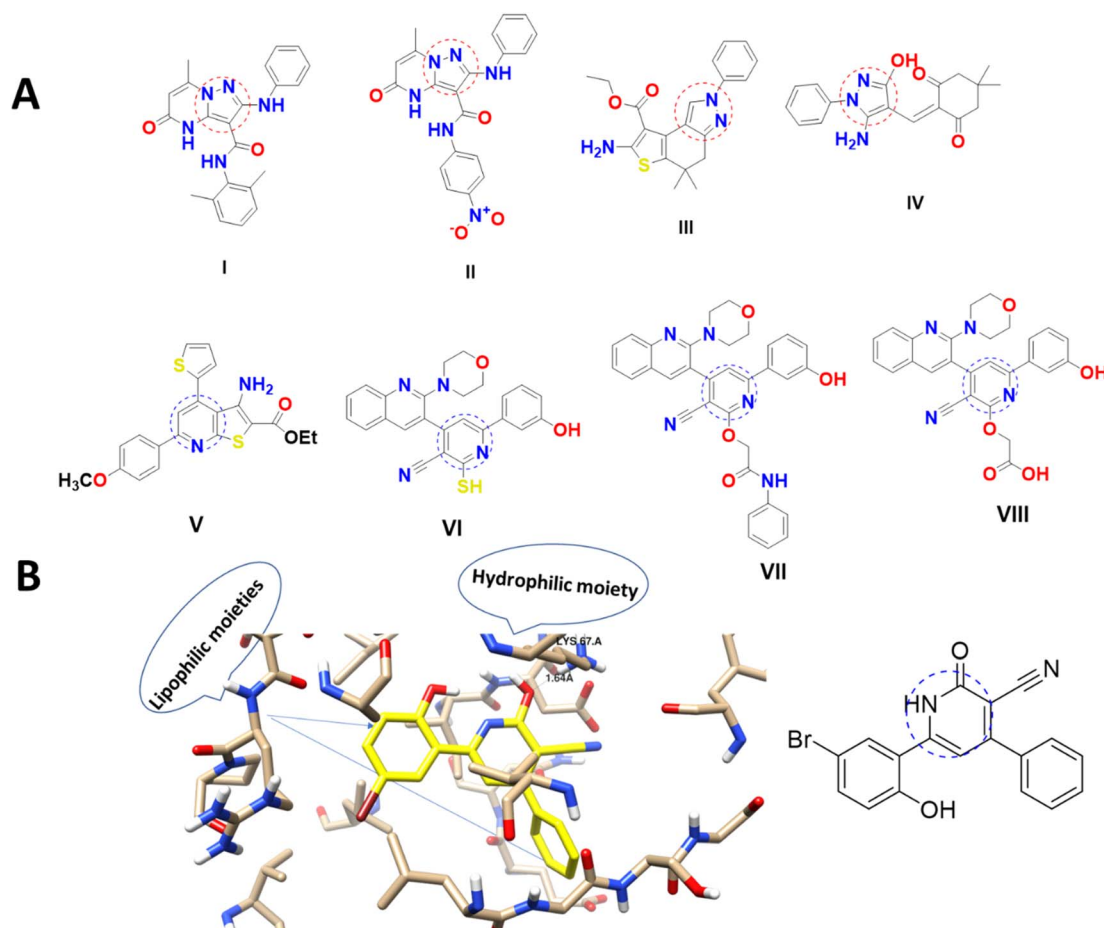


Fig. 1 (A) Pyrazole and cyanopyridine derivatives as PIM-1 kinase inhibitors^{18–23} and (B) molecular visualization of the PIM-1 active site (PDB ID = 2OBJ) with cyanopyridine inhibitor.²⁴



properties of the pyridine scaffold can be improved by incorporating pyrazolyl, Mannich bases, and acetyl hydrazide at C2 center of the pyridine nucleus. Hydrazide moiety was reported to enhance hydrogen bonding potential with the kinase active site and modulate the pharmacokinetics of drugs.²⁹

The performed structural analysis, together with the results of the biological tests, show that cyanopyridine could potentially be an efficient liver cancer therapeutic compound. Focusing on the molecular mechanism of action of cyanopyridine specifically for liver cancer provides insight into the possible therapeutic effect of this compound. Furthermore, the obtained data can be used for further development of cyanopyridine as a safe and effective liver cancer therapeutic strategy. In continuation of our research line, our current research interests aim at developing novel pyridine and pyrazolyl pyridine conjugates with potent cytotoxicity against liver cancer cells and identifying the molecular target and effective cell death mechanism.^{30–33}

2 Results chemistry

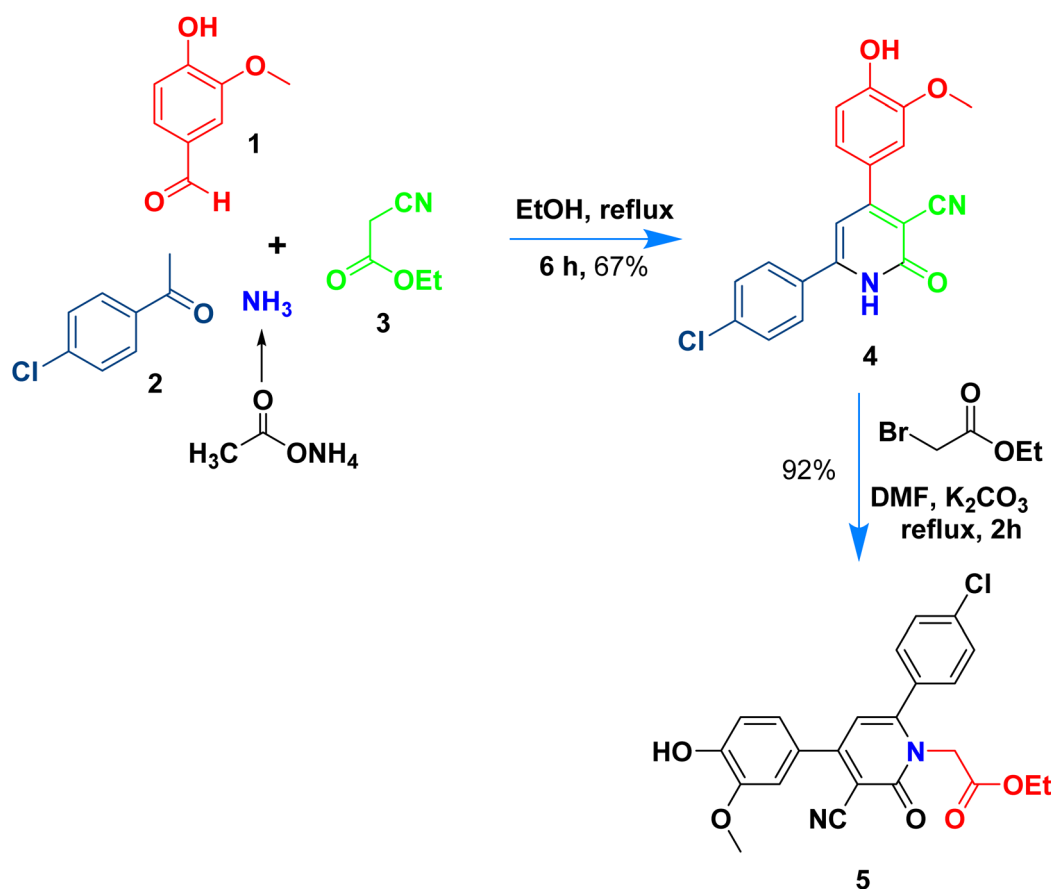
The present work aims to prepare a new series of 2-oxo-nicotinonitrile derivatives such as *N*-alkylated, Mannich bases, and pyrazolyl analogues. The preparation of 2-pyridone derivative **4** is the main point in the work, where it is synthesized *via* one-pot condensation of vanillin, 4-chloroacetophenone, ethyl

cianoacetate in the presence of ammonium acetate^{11,12,34} (Scheme 1). The reaction proceeded at reflux temperature in acetic acid for 6 hours, and the product's structure agreed with its spectral data (IR, ¹H, and ¹³C NMR). Nicotinonitrile **4** was subjected to an alkylation reaction with ethyl bromo acetate in the presence of potassium carbonate to afford the respective *N*-alkylated analogue. The reaction smoothly proceeds at room temperature for two hours and gives a good yield (92%). The presence of lactam carbonyl (N–C=O) at 1645 cm^{−1} confirmed the formation of an *N*-alkylated isomer.

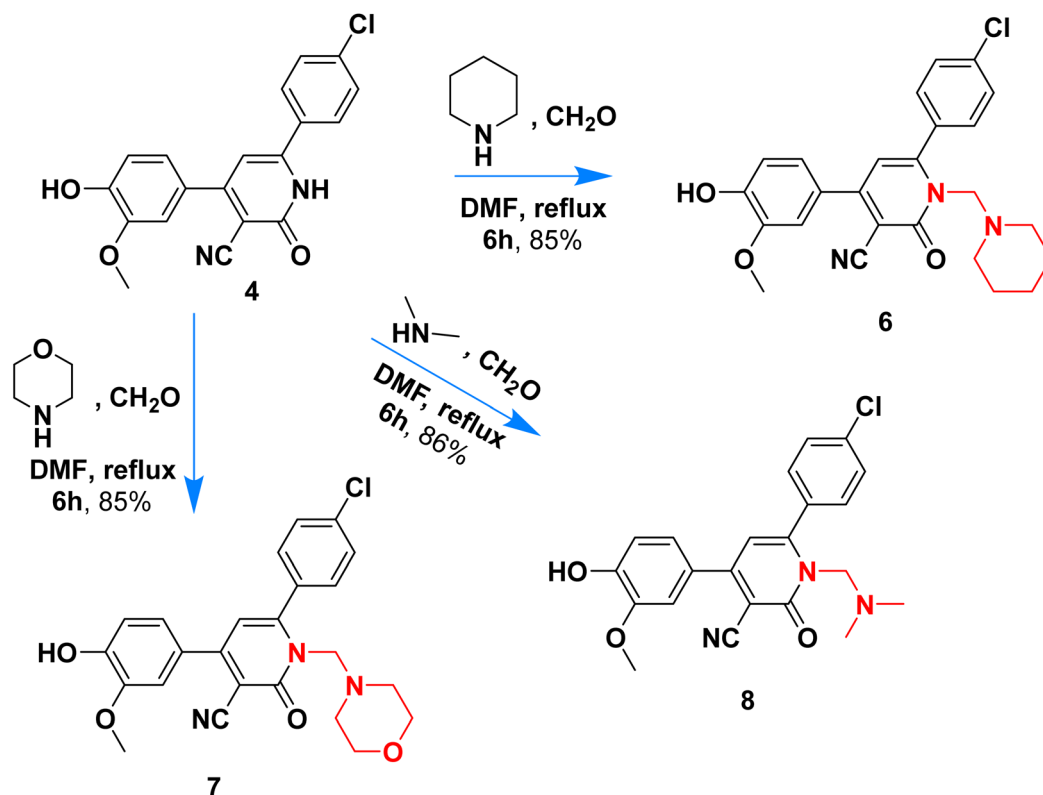
Scheme 2 outlined the Mannich reaction of nicotinonitrile **4** with piperidine, morpholine, and dimethyl amine in formaldehyde. The Mannich compounds are formed under heating for 8 hours and isolated in good yields (85 and 86%). Compound **8** contains bands at 3484, 2196, and 1646 cm^{−1} for OH, CN, and C=O functions. Its ¹H NMR confirmed the presence of NCH₂N–protons at 3.60 ppm as a singlet peak, and the piperidine protons appeared at δ_H 1.20, 1.50, and 1.60 ppm as two multiplet and triplet.

Its ¹³C NMR spectrum accounted for 19 signals at δ_C 18.55, 28.20, 53.13, 55.81, 56.02, 106.4, 112.5, 115.5, 117.0, 121.8, 126.5, 128.8, 129.6, 135.8, 147.5, 149.1, 149.7, 159.4, 162.3 for sp³, sp², sp carbons.

Hydrazinolysis of ester **5** with hydrazine hydrate followed by heterocyclization with acetyl acetone, ethyl acetoacetate, and



Scheme 1 Synthetic route of *N*-alkylated nicotinonitrile **5**.



Scheme 2 Mannich type reaction of nicotinonitrile 4.

ethyl cyanoacetate afforded the respective pyrazolyl **10–12** in 75–88% yield (Scheme 3). The formation of pyrazolyl derivatives was performed under reflux for 6 hours in ethanol, and the products were obtained in high yield (above 75%). Hydrazide **6** contains two adjacent nucleophilic centers (NH-NH_2) that enable such compound to act as a key precursor for the synthesis of different five-membered rings *via* its reaction with 1,3-dielectrophiles.

The chemical structure of pyrazolyl derivatives **10–12** was confirmed from spectral analysis, for example, the IR spectrum of 6-(4-chlorophenyl)-1-(2-(3,5-dimethyl-1*H*-pyrazol-1-yl)-2-oxoethyl)-4-(4-hydroxy-3-methoxyphenyl)-2-oxo-1,2-dihydropyridine-3-carbonitrile (**10**) showed main bands at 3337, 2210, 1686 cm^{-1} for OH, $\text{C}\equiv\text{N}$ and $\text{C}=\text{O}$. Its ^1H NMR spectrum, has a signal at 1.72, 2.05 ppm as two singlets for two methyl-attached pyrazole, two singlets at 3.83 and 5.14 for OCH_3 and NCH_2CO , and the pyridine pyrazole and aromatic protons appeared at the expected field at 6.93–6.95, 6.96–9.98, 7.23–7.25, 7.33–7.38, 7.59–7.61, and 7.91–7.93 ppm, in addition to phenolic hydroxide group appears at 9.73 ppm. The ^{13}C NMR data assigned 23 peaks at 13.68, 14.16, 51.81, 55.73, 90.55, 111.4, 113.7, 114.1, 116.2, 120.4, 122.0, 128.7, 128.9, 129.0, 129.2, 134.0, 135.4, 137.6, 147.3, 147.7, 155.0, 163.1, 168.3 for sp^3 , sp^2 , sp carbons.

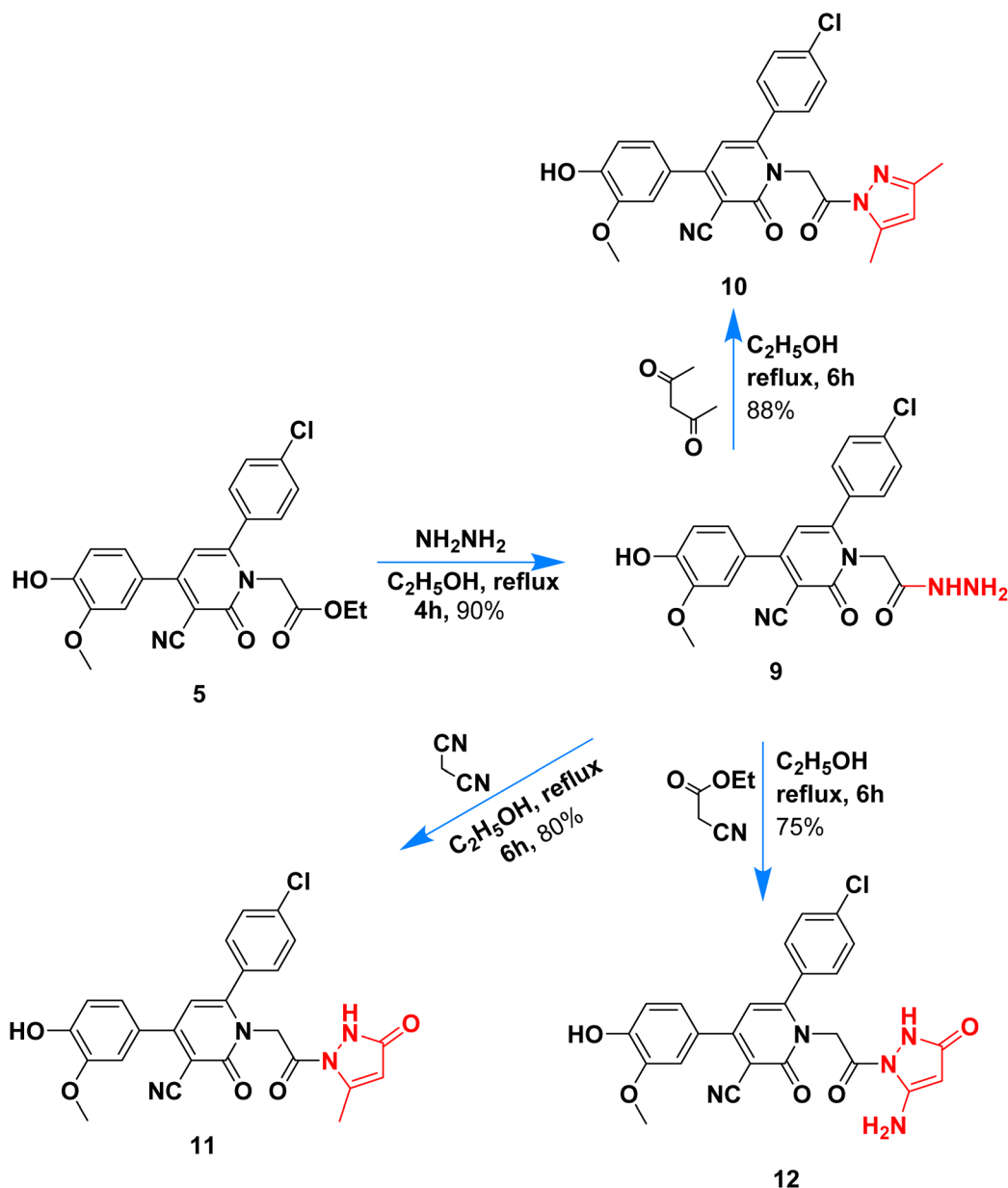
2.1 Biological investigations

2.1.1 Compound 9 exhibited potent cytotoxicity in HepG2 cancer cells. The cytotoxicity of the synthesized compounds

against HepG2 and MCF-7 cells was assessed using the MTT assay. Compared to staurosporine ($\text{IC}_{50} = 6.76 \mu\text{M}$), compounds **5**, **9**, and **10** showed potent cytotoxicity against MCF-7 cells (IC_{50} values of 4.15, 0.34, and 2.14 μM , respectively) as shown in Table 1. Furthermore, with IC_{50} values of 2.19, 0.18, and 3.47 μM , they demonstrated potent cytotoxicity against HepG2 cells. Other compounds exhibited encouraging cytotoxicity against both cell lines. According to the data presented in Fig. 2 for the cell viability dose–response curve of compound **9** against cancer cells of MCF-7, HepG2, and normal THLE2 cells, compound **9** was tested at various concentrations. Compound **9** exhibited a potent percentage of cell growth by 96%, and 94%, respectively; while the maximum cell growth inhibition against the normal cells was 13%, these values agreed with the IC_{50} values. At its maximal concentration, it increased the proportion of cancer cells that could survive, during which time normal cell viability wasn't much affected; this brought to light compound **9**'s selectivity profile.

Correlating the compounds' differential activity patterns to their corresponding structural features has been considered helpful in highlighting key structural requirements for cytotoxic activity. It is worth noting that the cytotoxic activity against the human breast (MCF-7) cancerous cell line favors polar functionality rather than hydrophobic ones. The latter has been demonstrated for introducing ethoxyacetyl, dimethyl amino, and hydrazide functionality at the compound structural diversity site. Compared to the unsubstituted lead compound (**4**), the activity patterns have increased from micromolar concentration





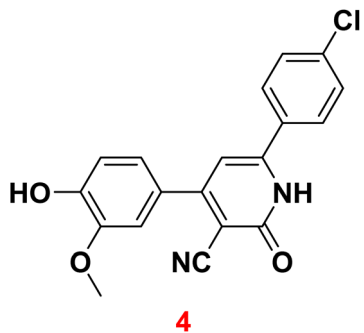
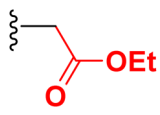
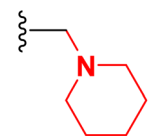
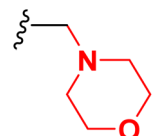
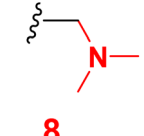
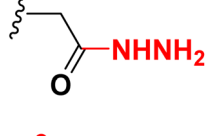
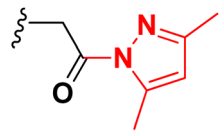
Scheme 3 Synthetic route of pyrazolyl nicotinonitriles 10–12.

(6.17 ± 0.32) to lower micromolar range for compounds 5 and 8 (4.15 ± 0.21 and 2.14 ± 0.1 , respectively) till reaching a sub-micromolar concentration for compound 9 (0.44 ± 0.01). Contrarily, the cytotoxic activity at MCF-7 was found intolerant to more hydrophobic substituents such as the cyclic aliphatic moieties (piperidine; 6 or morpholine; 7) as well as the heteroaromatic scaffold (pyrazole ring; 10). The MCF-7 depicted activity patterns have also been consistent with those at the hepatic (HepG2) cancerous cell line where top activity IC_{50} s were assigned to the compounds with many polar substitutions (compounds 5, 8, and 9). The later structure–cytotoxic relationship is quite in line with the current literature, where the introduction of polar scaffolds with relevant hydrogen bond potentiality (hydrogen bond donor and/or acceptor) has been

associated with improved pharmacokinetic properties, particularly the dissolution and distribution patterns.³⁵ Moreover, polar scaffolds have been reported with the merits of mediating key polar contacts with target sites resulting in better binding affinity and improved pharmacodynamic profiles.³⁶

To better acknowledge the polar potentiality of the synthesized compounds, we have deduced more relevant bioactivity indicators that consider both compounds' polarity and lipophilicity indices. Physiochemical properties of compounds like hydrogen bond acceptor/donor (number of heteroatoms) and structural-related lipophilic characteristics ($\log P$) are best accounted within the estimation of ligand's efficiencies (LEs) and lipophilic efficiencies (LLEs) bioactivity indices.³⁷ Typically, compound with promising activity profiles have been reported

Table 1 Cytotoxicity of tested compounds against MCF-7 and HepG2 cancer cells using the MTT assay

	IC ₅₀ ± SD ^a	
	MCF-7	HepG2
 4	6.17 ± 0.32	7.38 ± 0.45
 5	4.15 ± 0.21	2.19 ± 0.18
 6	25.4 ± 0.9	≥50
 7	≥50	14.1 ± 0.6
 8	2.14 ± 0.1	3.47 ± 0.2
 9	0.44 ± 0.01	0.28 ± 0.01
 10	≥50	21.6 ± 1.1

^a IC₅₀ values are expressed in mean ± SD of three independent trials.

with LE and LLE values above the 0.2 and 2, respectively.^{38,39} In the case of our synthesized compounds, compounds with incorporated higher polar functionality were assigned with the

relevant LE and LLE indices (Fig. 3). Notably, compounds 5 and 8 harboring the ethoxyacetyl and dimethyl amino groups showed LE; LLE of 0.29; 2.65 and 0.27; 2.97 at MCF-7 and 0.31; 2.93 and 0.26; 2.76 at HepG2 respectively, whereas compound 9 was estimated with the best LE; LLE values (0.29; 5.41 at MCF-7 and 0.30; 5.60 at HepG2). The later efficiency indices further highlight the advent of incorporating the polar functionalities for cytotoxic activity of these synthesized pyridine and pyrazolyl pyridine conjugates. Fig. 4 summarizes the process of generating the suggested SAR model. In counting for the advent of polar functionality for improving the compound's pharmacokinetic and pharmacodynamics profile has been also proceeded throughout the following sections. An investigation for tampered pharmacokinetics was evaluated through the *in silico* solubility profile prediction while as molecular docking simulation was adopted to assess the potential ligand binding affinity.

2.1.2 Compound 9 induced potent PIM-1 kinase inhibition. Compounds 5, 9, and 10 were tested for their inhibitory effects against PIM-1 to determine their molecular targets. Table 2 shows that the investigated drugs inhibited PIM-1 kinase activity, which is encouraging; intriguingly, the IC₅₀ values for compound 9 were 8.4 nM, resulting in a 98.8% inhibition, in contrast to staurosporine, which had an IC₅₀ value of 16.7 nM and an inhibition of 95.6% and the previously synthesized compound “pyrido[2,3-*d*] pyrimidine-6-carbonitrile with IC₅₀ value of 11.4 nM. Further, compounds 5 and 10 showed encouraging PIM-1 inhibition, with IC₅₀ values of 64.6 nM and 34.6 nM, respectively, and inhibitory activity of 83.4% and 87.6%. These results agreed with previous literature on discovering potent pyridine and pyrazolyl derivatives inhibiting PIM kinase in liver cancer.^{41–44} As a result, we are focusing on creating new and effective pyridine and pyrazolyl pyridine conjugates to inhibit PIM-1 kinase.

2.1.3 Compound 9 induced caspase 3, 8, 9 activation in HepG2 cancer cells. As a characteristic of cell death, caspase activation can be measured in cellular experiments to identify the factors that trigger or impede the “death cascade.” The most active compound 9 was evaluated for activity on caspases in treated HepG2 at the IC₅₀ dose. Results, as shown in Table 3, revealed that compound 9 upregulated caspase 3, 8, and caspases 9 levels by 9.8, 74.4, and 112.6 [ng mL^{−1}], respectively, compared to the control. Notably, it demonstrated significantly higher selectivity for caspase-9 compared to caspase-3 and caspase-8 by almost 2.6-fold. So, the data showed that compound 9 might induce cell death in HepG2 cancer cells.

2.1.4 Compound 9 induced apoptosis in HepG2 cancer cells. Using flow cytometric examination of Annexin V/PI staining, the apoptotic cell death in both untreated and treated HepG2 cells was investigated to assess compound 9's apoptotic activity (IC₅₀ = 0.28 μM, 48 h). Fig. 5 shows that compound 9 caused a significant increase in apoptotic cell death in HepG2 cells, with a total apoptotic cell death 175 times higher than in the untreated control group (0.30%). Compound 9 also caused 52.7% apoptosis, with 37.5% of cell death occurring during late apoptosis and 15.2% during early



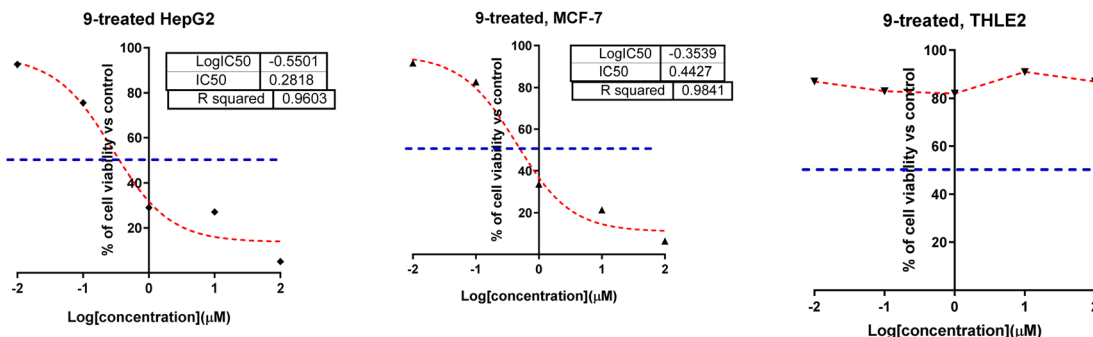


Fig. 2 Dose–response non-linear regression curve fitting the percentage of cell viability of HepG2, MCF-7, and THLE2 cells vs. log[con. μM], R square ≈ 1 using the GraphPad prism.

apoptosis. Nevertheless, when it came to evaluating necrosis, compound 9 therapy failed to enhance necrosis cell death.

It was also reported^{45–48} that caspase activation plays a central role in the execution of apoptosis as programmed cell death. Caspases 3, 8 and 9 are mainly incorporated in extrinsic and intrinsic pathways. So, Apoptotic cell death can be defined as caspase cascade activators.

Taken together, cyanopyridine–pyrazole conjugates exhibited potent anti-cancer activity *in vitro* against liver cancers. A target identification study revealed a potential protein tyrosine kinase (PTK) as the mode of action of cyanopyridine. Furthermore, the compound directly exhibited potent PIM-1 kinase inhibition, leading to apoptosis of liver cancer cells. This study concludes that cyanopyridine, as an anti-cancer small molecule, is a PIM-1 kinase inhibitor and can be considered as a promising lead for the development of more potent anti-cancer compounds.

2.2 In silico studies

2.2.1 Molecular docking. The docking of compound 9 within the PIM-1 binding site, with the same binding mechanism as the co-crystallized ligand, is illustrated in Fig. 6. According to the docking results, the molecule was correctly positioned inside the PIM-1 active site with a binding energy of -21.94 kcal mol⁻¹ compared to the crystallized ligand with a binding energy of -19.57 kcal mol⁻¹. Additionally, the binding energy of compound 9 was compared to a previously published⁴⁹ compound that exhibited -20.84 kcal mol⁻¹. Compound 9 also formed three stable hydrogen bond interactions with the amino acids Lys67, Glu171, and Asp 186, with bond lengths of 1.88, 1.28, and 2.14 Å, respectively. The advent of incorporating the polar functionality (hydrazide scaffold) in compound 9 for significant pharmacodynamic profiling has been highlighted with mediated hydrogen bonding for this group with pocket polar lining residues. Additionally, 4-chloro phenyl ring exhibited promising lipophilic interactions with the nonpolar amino acids, including Leu 120 and Val 52. These drug–target interactions stabilize the drug in the conformation required for proper binding to the receptor.

As summarized in Table 4, in contrast with other compounds that exhibited less binding affinities with lower binding energies ranging from -9.34 kcal mol⁻¹ to -12.76 kcal mol⁻¹ and less

interactions with the key amino acids of protein active sites, in agreement with experimental results of PIM-1 kinase inhibition.

It appears that the efficient target for apoptosis-mediated cell death is PIM-1 kinase inhibition, and the experimental enzyme target activity was supported by the molecular docking investigation.

2.2.2 Physicochemical and pharmacokinetic properties.

The promising compounds 5, 9, and 10 were investigated for their physicochemical and drug-likeness properties. As seen in Table 5, their results were encouraging according to Lipinski's five-rule model, which includes "molecular weight, number of rotatable bonds, H-bond donor, and acceptors along with a number of violations." This applies especially to compound 9. Notably, compound 9 has been predicted with the highest solubility index (1036.43 mg L⁻¹), the thing that further highlights the advent of incorporating the polar hydrazide functionality for improving the compound's pharmacokinetic (dissolution) profile.

3 Experimental

Melting points were detected using an Electro-thermal IA 9100 apparatus. IR spectra (KBr) were recorded on a Nexus 670 FTIR Nicolet, Fourier transform infrared spectrometer. The ¹H and ¹³C NMR spectra were measured in DMSO-d₆ with a JEOL-JNM-LA 400 MHz spectrometer and 100 MHz for ¹³C NMR. The chemical shifts are expressed on the δ (ppm) scale using TMS as the standard reference. TLC was performed on Merck Silica Gel 60F254 and detected by UV light. Elemental analysis measured on a PerkinElmer 240 (microanalysis), Microanalysis Center, Cairo University.

3.1 6-(4-Chlorophenyl)-4-(4-hydroxy-3-methoxyphenyl)-2-oxo-1,2-dihydropyridine-3-carbonitrile (4)

A mixture of 4-hydroxy-3-methoxybenzaldehyde (vanillin) (1) (0.02 mole) and 4-chloroacetophenone (2) (0.02 mole) and ethyl cyanoacetate (3) (0.02 mole) in the presence of ammonium acetate (0.16 mole) with acetic acid (20 mL) was heated under reflux (6 hours). After cooling, the resulting solid was filtered off and dried. Pale yellow solid (AcOH), mp = 340–342 °C, yield: 67%. IR spectrum, ν , cm⁻¹: 3483 (OH and NH), 2226 (C≡N),



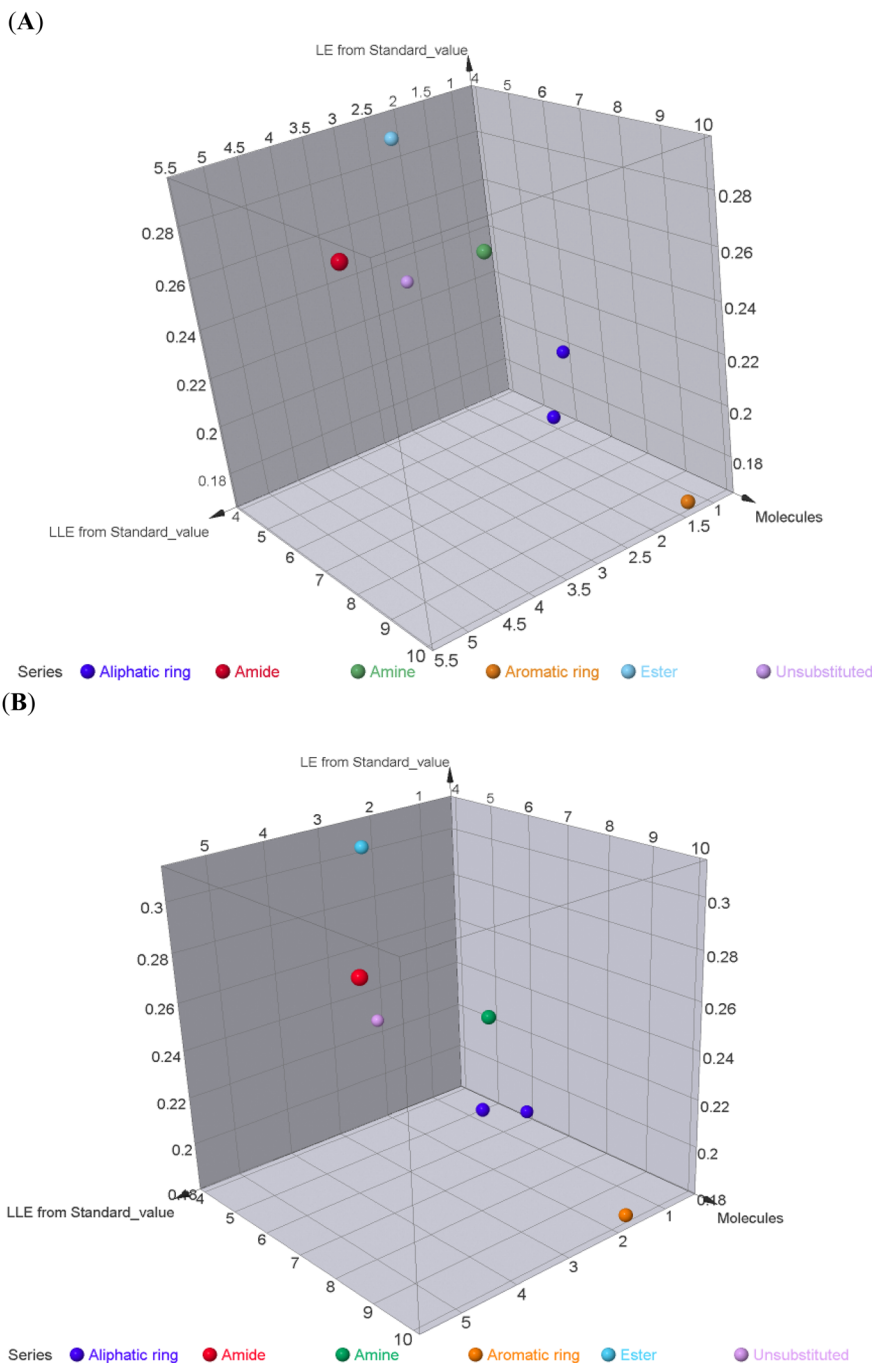


Fig. 3 Three-dimensional charts for estimated compounds' LE and LLE indices being calculated from incorporating the compounds' polarity and lipophilicity characteristics within the obtained cytotoxicity IC_{50} values against MCF-7 (A) and HepG2 (B) cancerous cell lines. Charts are constructed via DataWarriors V6.2.5 software.

1645 (C=O), 822 (C-Cl). 1H NMR spectrum, δ , ppm: 3.85 (s, 3H, OCH_3), 6.85 (s, 1H, $H_{pyridine}$), 6.92–6.94 (d, 1H, $^3J = 8.0$ Hz, H_{aryl}), 7.22–7.24 (d, 1H, $^3J = 6.40$ Hz, H_{aryl}), 7.25 (s, 1H, H_{aryl}), 7.57–7.59 (d, 2H, $^3J = 8.8$ Hz, H_{aryl}), 7.89–7.91 (d, 2H, $^3J = 8.80$ Hz, H_{aryl}), 9.75 (s, 1H, OH), 12.66 (s 1H, NH). ^{13}C NMR spectrum, δ_C , ppm: 104.9, 112.1, 115.3, 116.8, 120.2, 122.7, 126.2, 128.7, 128.9, 135.5, 147.1, 149.3, 157.4, 159.4, 160.2 (sp^3 , sp^2 , sp carbons), found, %: C, 64.78; H, 3.66; N, 8.00. Calculated, $C_{19}H_{13}ClN_2O_3$ (352.77) %: C, 64.69; H, 3.71; N, 7.94.

3.2 Ethyl 2-(6-(4-chlorophenyl)-3-cyano-4-(4-hydroxy-3-methoxyphenyl)-2-oxo pyridin-1(2H)-yl)acetate (5)

A mixture of 6-(4-chlorophenyl)-4-(4-hydroxy-3-methoxyphenyl)-2-oxo-1,2-dihydropyridine-3-carbonitrile (**1**) (0.01 mole) and ethyl cyanoacetate (0.01 mole) in the presence of potassium carbonate in DMF (20 mL) was stirring at room temperature for 2 hours. The reaction mixture was diluted with HCl, and the formed solid was filtered off. Pale yellow solid (EtOH), mp =



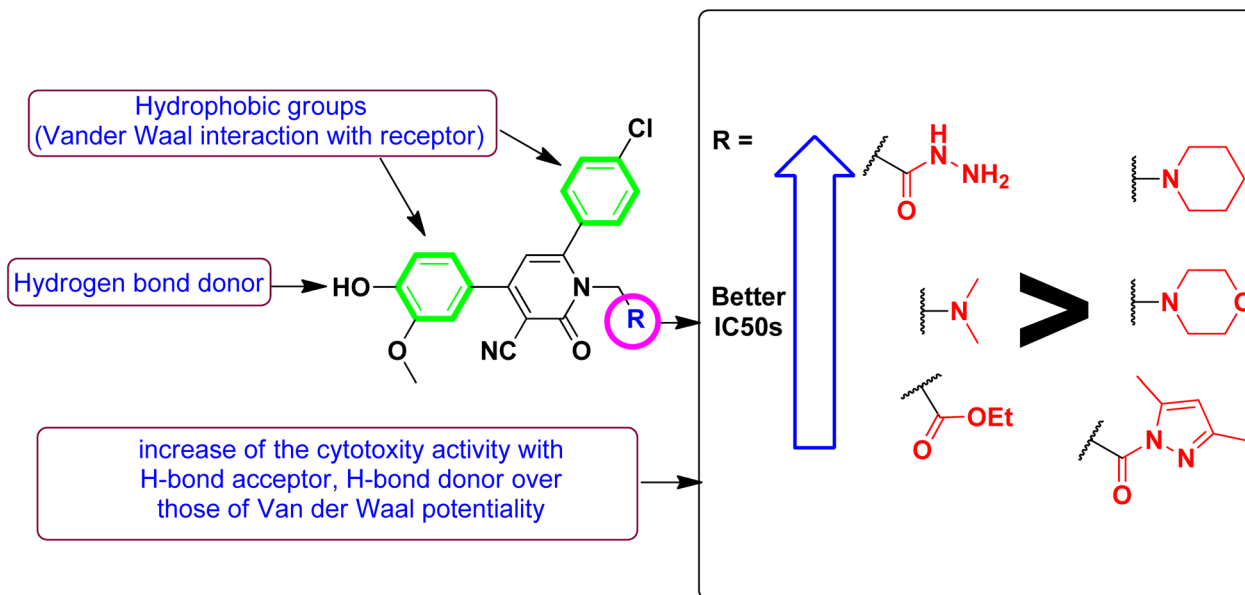


Fig. 4 Substituents anchored on the main scaffold with cytotoxic activities of the designed derivatives.

Table 2 IC₅₀ values of PIM-1 kinase inhibition of the most cytotoxic compounds

Compound	% of PIM-1 inhibition	IC ₅₀ ± SD ^a (nM)
5	83.4 ± 2.3	64.6 ± 0.2
9	98.8 ± 1.9	8.4 ± 0.2
10	87.6 ± 3.2	34.6 ± 0.12
Pyrido[2,3- <i>d</i>] pyrimidine-6-carbonitrile	97.8 ± 1.8	11.4 ± 0.13 (ref. 40)
Staurosporine	95.6 ± 2.4	16.7 ± 0.32

^a Values are expressed as an average of three independent replicates. "IC₅₀ values were calculated using sigmoidal non-linear regression curve fit of percentage inhibition against five concentrations of each compound".

292–294 °C, yield: 92%. IR spectrum, ν , cm⁻¹: 3485 (OH), 2222 (C≡N), 1750, 1683 (2C=O). ¹H NMR spectrum, δ , ppm: 1.16–1.20 (t, 3H, H_{ethyl}), 3.88 (s, 3H, OCH₃), 4.15–4.20 (q, 2H, H_{ethyl}), 5.13 (s, 2H, CH₂), 6.95–6.97 (d, 1H, ³J = 8.0, Hz, H_{aryl}), 7.23–7.25 (d, 1H, ³J = 8.0, Hz, H_{aryl}), 7.36 (s, 1H, H_{aryl}), 7.57–7.59 (d, 2H, ³J = 8.80, Hz, H_{aryl}), 7.86 (s, 1H, H_{pyridine}), 8.16–8.18 (d, 2H, ³J =

8.80, Hz, H_{aryl}), 9.72 (s, 1H, OH). Found, %: C, 62.95; H, 4.36; N, 6.38. Calculated, C₂₃H₁₉ClN₂O₅ (438.86) %: C, 62.95; H, 4.36; N, 6.38.

3.3 6-(4-Chlorophenyl)-4-(4-hydroxy-3-methoxyphenyl)-2-oxo-1-(piperidin-1-ylmethyl)-1,2-dihydropyridine-3-carbonitrile (6)

A mixture of 6-(4-chlorophenyl)-4-(4-hydroxy-3-methoxyphenyl)-2-oxo-1,2-dihydro pyridine-3-carbonitrile (4) (0.01 mole), (2 mL) formaldehyde (0.01 mole) and piperidine (0.01 mole) in DMF

Table 3 Concentrations of caspases 3, 8 and 9 (ng mL⁻¹) by ELISA in the untreated and 9-treated HepG2 cells

Compound	Concentration ^a [ng mL ⁻¹]		
	Caspase 3	Caspase 8	Caspase 9
9-Treated HepG2	9.8 ^b ± 0.9	74.4 ^b ± 2.2	112.6 ^b ± 2.9
Control	4.01 ± 0.21	55.01 ± 1.19	43.33 ± 0.49

^a Values are expressed as mean ± SD of three independent trials. ^b ($P \leq 0.05$) significantly different between treated and treated groups using GraphPad prism.

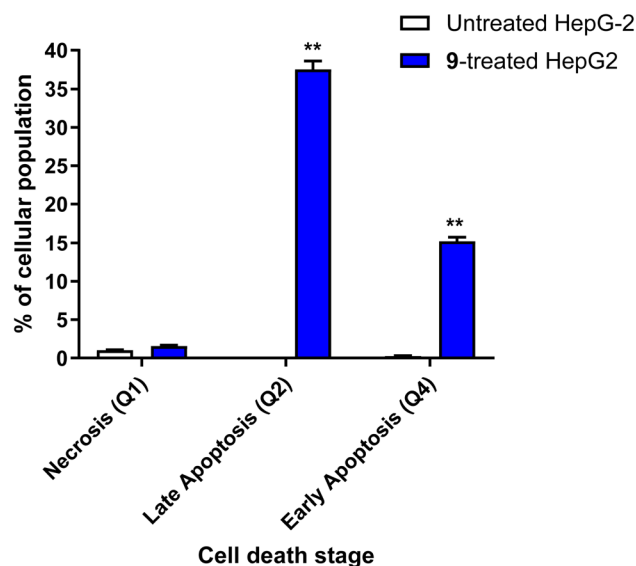


Fig. 5 Bar chart of apoptosis and necrosis assessment using Annexin V/PI staining of untreated and 9-treated HepG2 cancer cells. **($P \leq 0.01$) significantly different between untreated and treated cells using the unpaired *t*-test using GraphPad prism. Annexin V/PI histograms are supported in the ESI.†



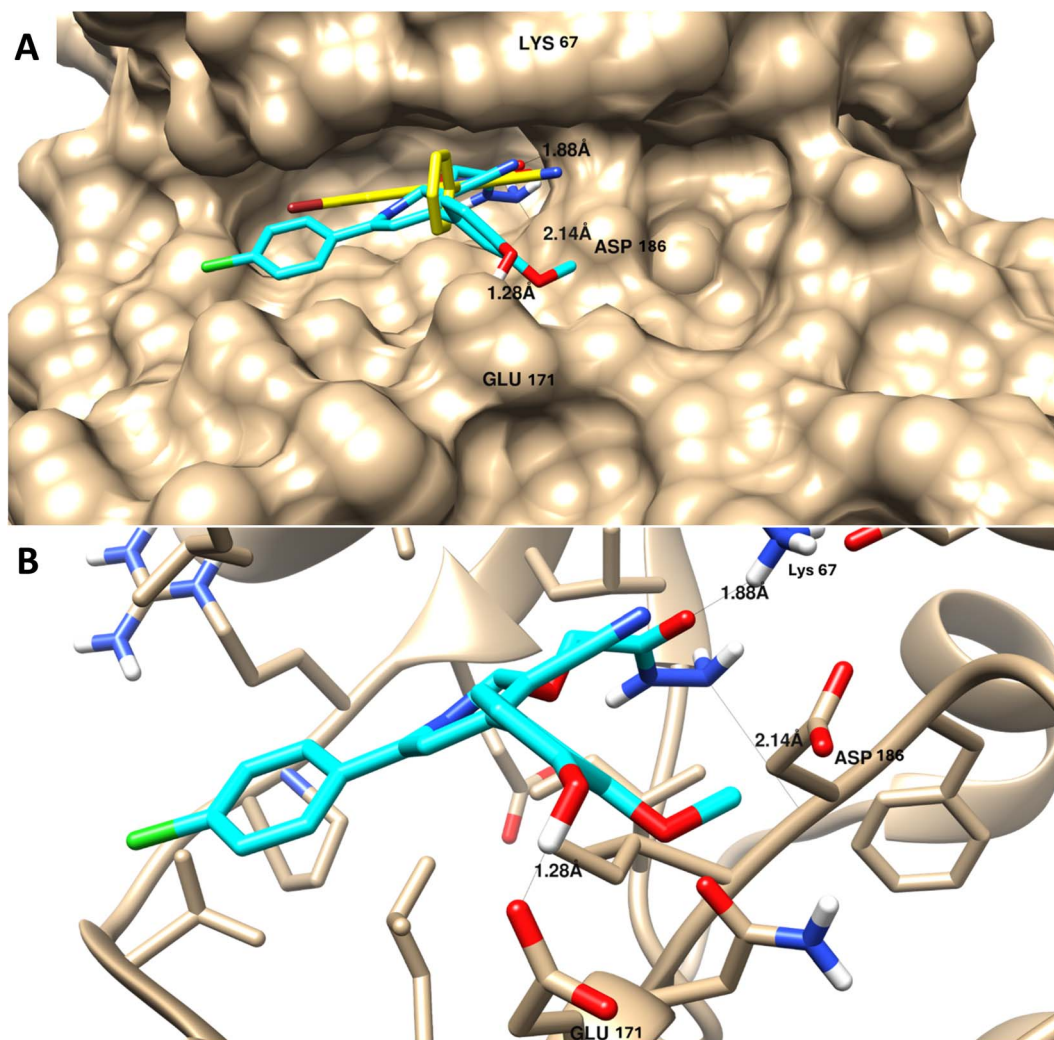


Fig. 6 Molecular docking of **9** towards PIM-1 protein (PDB = 2OBJ). (A) Surface disposition of the co-crystallized ligand (yellow-cored) and the docked compound (cyan-colored) and (B) interactive view of the compound with the highlighted key amino acids. 3D images were generated by Chimera-UCSF software.

(20 mL) was heated under reflux (8 hours). After cooling, the resulting solid was filtered off and dried. Pale yellow solid (EtOH), mp = 310–312 °C, yield: 85%. IR spectrum, ν , cm^{-1} : 3484 (OH), 2196 ($\text{C}\equiv\text{N}$), 1646 ($\text{C}=\text{O}$). ^1H NMR spectrum,

δ , ppm: 1.20 (m, 2H, H_{pip}), 1.50 (m, 4H, H_{pip}), 1.60 (t, 2H, H_{pip}), 3.85 (s, 3H, OCH_3), 3.75 (s, NCH_2N), 6.86 (s, 1H, $\text{H}_{\text{pyridine}}$), 6.92–9.94 (d, 1H, $^3J = 8.0$, Hz, H_{aryl}), 7.23–7.25 (dd, 1H, $^2J = 2.0$, $^3J = 8.40$, Hz, H_{aryl}), 7.33–7.34 (d, 1H, $^2J = 2.0$ Hz, H_{aryl}), 7.58–7.60

Table 4 Summary of ligand–receptor interaction with binding energies

Compounds	Binding affinities ^a	
	Binding energy (kcal mol^{-1})	Binding interactions
Co-crystallized ligand	−19.57	1 H-bond with Lys 67
4	−9.34	1 H-bond with Lys 67
5	−10.12	1 H-bond with Lys 67
6	−11.25	1 H-bond with Asp 196
7	−12.23	1 H-bond with Glu 171
8	−12.76	1 H-bond with Lys 67
9	−20.84	3 H-bond with Lys 67, Asp 196, and Glu 171
10	−11.98	1 H-bond with Lys 67

^a Binding affinities were calculated from docking results by AutoDock Vina with Chimera.



Table 5 Molecular properties and ADME pharmacokinetics of the promising compounds^a

#	Molsoft										SwissADME
	HBA	HBD	Solubility (mg L ⁻¹)	Drug score	M. wt (D)	MV (Å ³)	PSA (Å ²)	log <i>p</i>	BBB score	Nviolations	Drug likeness (Lipinski Pfizer filter)
5	6	1	72.27	-0.09	438.10	464.16	76.96	3.65	3.17	0	Yes
9	6	5	1036.43	0.78	426.11	432.93	108.99	1.69	2.22	0	Yes
10	5	1	126.13	0.46	409.12	443.85	62.11	3.45	4.4	0	Yes

^a M. wt: molecular weight, MV: molecular volume, PAS: polar surface area, log *p*: log *P*: octanol-water partition coefficient, nrotb: number of rotatable bonds, nviolations: number of violations, HBA: hydrogen bond acceptor, HBD: hydrogen bond donor, drug-likeness score, compounds having negative, or zero value should not be considered as drug-like". Drug likeness (Lipinski Pfizer filter)/"Yes, drug-like" MW ≤ 500, log *p* ≤ 4.25, HBA ≤ 10 and HBD ≤ 5.⁴⁰

(dd, 2H, ²*J* = 1.60, ³*J* = 6.80, Hz, H_{aryl}), 7.90–7.93 (d, 2H, ³*J* = 8.80, Hz, H_{aryl}), 9.73 (s, 1H, OH). ¹³C NMR spectrum, δ_C, ppm: 18.55, 28.20, 53.13, 55.81, 56.02, 106.4, 112.5, 115.5, 117.0, 121.8, 126.5, 128.8, 129.6, 135.8, 147.5, 149.1, 149.7, 159.4, 162.3 (sp³, sp², sp carbons). Found, %: C, 66.66; H, 5.35; N, 9.40 and calculated, C₂₅H₂₄ClN₃O₃ (449.94) %: C, 66.74; H, 5.38; N, 9.34.

3.4 6-(4-Chlorophenyl)-4-(4-hydroxy-3-methoxyphenyl)-1-(morpholinomethyl)-2-oxo-1,2-dihydropyridine-3-carbonitrile (7)

A mixture of 6-(4-chlorophenyl)-4-(4-hydroxy-3-methoxyphenyl)-2-oxo-1,2-dihydro pyridine-3-carbonitrile (**4**) (0.01 mole), (2 mL) formaldehyde (0.01 mole) and morpholine (0.01 mole) in DMF (20 mL) was heated under reflux (8 hours). After cooling, the resulted solid was filtered off and dried. Pale yellow solid (EtOH), mp = 332–334 °C, yield: 85%. IR spectrum, ν, cm⁻¹: 3484 (OH), 2201 (C≡N), 1645 (C=O). ¹H NMR spectrum, δ, ppm: 2.54 (d, 4H, H_{morph}), 3.40 (d, 4H, H_{morph}), 3.76 (s, NCH₂N), 3.85 (s, 3H, OCH₃), 6.86 (s, 1H, H_{pyridine}), 6.92–9.94 (d, 1H, ³*J* = 8.40, Hz, H_{aryl}), 7.23–7.25 (dd, 1H, ²*J* = 2.0, ³*J* = 8.40, Hz, H_{aryl}), 7.33–7.34 (d, 1H, ²*J* = 2.0 Hz, H_{aryl}), 7.58–7.59 (dd, 2H, ²*J* = 2.40, ³*J* = 8.40, Hz, H_{aryl}), 7.90–7.92 (d, 2H, ³*J* = 8.40, Hz, H_{aryl}), 9.72 (s, 1H, OH). ¹³C NMR spectrum, δ_C, ppm: 36.0, 42.3, 48.0, 55.82, 106.2, 112.5, 115.5, 116.9, 121.8, 126.5, 128.8, 129.8, 129.6, 131.4, 135.8, 147.5, 149.1, 159.4, 162.3 (sp³, sp², sp carbons). Found, %: C, 63.88; H, 4.94; N, 9.27, calculated, C₂₄H₂₂ClN₃O₄ (451.91) %: C, 63.79; H, 4.91; N, 9.30.

3.5 6-(4-Chlorophenyl)-1-((dimethylamino)methyl)-4-(4-hydroxy-3-methoxyphenyl)-2-oxo-1,2-dihydropyridine-3-carbonitrile (8)

A mixture of 6-(4-chlorophenyl)-4-(4-hydroxy-3-methoxyphenyl)-2-oxo-1,2-dihydro pyridine-3-carbonitrile (**4**) (0.01 mole), (2 mL) formaldehyde (0.01 mole) and dimethylamine (0.01 mole) in DMF (20 mL) was heated under reflux (8 hours). After cooling, the resulting solid was filtered off and dried. Pale yellow solid (EtOH), mp = 302–304 °C, yield: 86%. IR spectrum, ν, cm⁻¹: 3485 (OH), 2210 (C≡N), 1646 (C=O). ¹H NMR spectrum, δ, ppm: 1.90 (s, 6H, H_{methyl}), 3.60 (s, NCH₂N), 3.85 (s, 3H, OCH₃), 6.87 (s, 1H, H_{pyridine}), 6.92–9.94 (d, 1H, ³*J* = 8.40, Hz, H_{aryl}), 7.23–7.25 (dd, 1H, ²*J* = 2.40, ³*J* = 8.40, Hz, H_{aryl}), 7.33–7.34 (d, 1H, ²*J* = 2.0 Hz, H_{aryl}), 7.59–7.61 (dd, 2H, ²*J* = 2.0, ³*J* = 6.80, Hz, H_{aryl}), 7.91–7.93 (d, 2H, ³*J* = 8.40, Hz, H_{aryl}), 9.72 (s, 1H, OH). ¹³C NMR

spectrum, δ_C, ppm: 18.55, 21.04, 48.59, 56.02, 92.01, 108.1, 112.5, 115.5, 116.9, 121.8, 126.5, 128.8, 129.6, 135.8, 147.5, 149.1, 159.5, 162.2 (sp³, sp², sp carbons). Found, %: C, 64.36; H, 4.89; N, 10.29, calculated, C₂₂H₂₀ClN₃O₃ (409.87) %: C, 64.47; H, 4.92; N, 10.25.

3.6 2-(6-(4-Chlorophenyl)-3-cyano-4-(4-hydroxy-3-methoxyphenyl)-2-oxopyridin-1(2H)-yl)acetohydrazide (9)

A mixture of ethyl 2-(6-(4-chlorophenyl)-3-cyano-4-(3-hydroxy-4-methoxyphenyl)-2-oxo pyridin-1(2H)-yl) acetate (**4**) (0.01 mole) and hydrazine hydrate (0.01 mole) with ethanol (20 mL) was heated under reflux (4 hours). After cooling, the resulting solid was filtered off and dried. Pale yellow solid (EtOH), mp = 226–228 °C, yield: 90%. IR spectrum, ν, cm⁻¹: 3286, 3203, 3130 (OH, NH, NH₂), 2212 (C≡N), 1663 (C=O). ¹H NMR spectrum, δ, ppm: 3.88 (s, 3H, OCH₃), 4.50 (bs, 1H, NH₂), 4.99 (s, 2H, CH₂), 6.97–6.99 (d, 1H, ³*J* = 8.40, Hz, H_{aryl}), 7.25–7.27 (d, 1H, ³*J* = 8.40, Hz, H_{aryl}), 7.36 (s, 1H, H_{aryl}), 7.57–7.59 (d, 2H, ³*J* = 8.40, Hz, H_{aryl}), 7.84 (s, 1H, H_{pyridine}), 8.22–8.24 (d, 2H, ³*J* = 8.40, Hz, H_{aryl}), 9.40 (s, 1H, OH), 9.70 (bs, 1H, NH). ¹³C NMR spectrum, δ_C, ppm: 55.93, 64.31, 92.28, 112.8, 113.9, 115.5, 121.8, 126.3, 128.8, 129.2, 129.5, 135.4, 148.8, 155.2, 156.5, 163.4 and 166.5 (sp³, sp², sp carbons). Found, %: C, 59.29; H, 4.00; N, 13.25. Calculated, C₂₁H₁₇ClN₄O₄ (424.84) %: C, 59.37; H, 4.03; N, 13.19.

3.7 6-(4-Chlorophenyl)-1-(2-(3,5-dimethyl-1H-pyrazol-1-yl)-2-oxoethyl)-4-(4-hydroxy-3-methoxyphenyl)-2-oxo-1,2-dihydropyridine-3-carbonitrile (10)

A mixture of 2-(6-(4-chlorophenyl)-3-cyano-4-(4-hydroxy-3-methoxyphenyl)-2-oxopyridin-1(2H)-yl) acetohydrazide (**6**) (0.01 mole) and acetyl acetone (0.01 mole) with ethanol (20 mL) absolute was heated under reflux (6 hours). After cooling, the reaction mixture was diluted with water, and the formed precipitate was filtered off. Pale yellow solid (EtOH), mp = 206–208 °C, yield: 88%. IR spectrum, ν, cm⁻¹: 3337 (OH), 2210 (C≡N), 1686 (C=O). ¹H NMR spectrum, δ, ppm: 1.72, 2.05 (2s, 6H, H_{pyrazole}), 3.83 (s, 3H, OCH₃), 5.14 (s, NCH₂CO), 6.93–6.95 (m, 2H, H_{pyridine} and pyrazole), 6.96–9.98 (d, 1H, ³*J* = 8.0, Hz, H_{aryl}), 7.23–7.25 (dd, 1H, ²*J* = 2.0, ³*J* = 8.0, Hz, H_{aryl}), 7.33–7.38 (d, 1H, ²*J* = 2.0 Hz, H_{aryl}), 7.59–7.61 (dd, 2H, ²*J* = 2.0, ³*J* = 8.40, Hz, H_{aryl}), 7.91–7.93 (d, 2H, ³*J* = 8.40, Hz, H_{aryl}), 9.73 (s, 1H, OH). ¹³C NMR spectrum, δ_C, ppm: 13.68, 14.16, 51.81, 55.73, 90.55, 111.4,



113.7, 114.1, 116.2, 120.4, 122.0, 128.7, 128.9, 129.0, 129.2, 134.0, 135.4, 137.6, 147.3, 147.7, 155.0, 163.1, 168.3 (sp³, sp², sp carbons). Found, %: C, 64.36; H, 4.89; N, 10.29, calculated, C₂₂H₂₀ClN₃O₃ (409.87) %: C, 64.47; H, 4.92; N, 10.25.

3.8 6-(4-Chlorophenyl)-4-(4-hydroxy-3-methoxyphenyl)-1-(2-(5-methyl-3-oxo-2,3-dihydro-1H-pyrazol-1-yl)-2-oxoethyl)-2-oxo-1,2-dihydropyridine-3-carbonitrile (11)

A mixture of 2-(6-(4-chlorophenyl)-3-cyano-4-(4-hydroxy-3-methoxyphenyl)-2-oxopyridin-1(2H)-yl) acetohydrazide (**6**) (0.01 mole) and ethyl acetoacetate (0.01 mole) with ethanol (20 mL) absolute was heated under reflux (6 hours). After cooling, the reaction mixture was diluted with water, and the formed precipitate was filtered off. Pale yellow solid (EtOH), mp = 206–208 °C, yield: 80%. IR spectrum, ν , cm⁻¹: 3321 (OH), 2224 (C≡N), 1692, 1671 (C=O). ¹H NMR spectrum, δ , ppm: 2.02 (s, 3H, H_{methyl}), 3.87 (s, 3H, OCH₃), 5.14 (s, NCH₂CO), 6.92–6.95 (m, 2H, H_{pyridine} and pyrazole), 6.96–6.98 (d, 1H, ³J = 8.0, Hz, H_{aryl}), 7.23–7.25 (dd, 1H, ²J = 2.0, ³J = 8.0, Hz, H_{aryl}), 7.33–7.38 (d, 1H, ²J = 2.0 Hz, H_{aryl}), 7.59–7.61 (dd, 2H, ²J = 2.0, ³J = 8.40, Hz, H_{aryl}), 7.91–7.93 (d, 2H, ³J = 8.40, Hz, H_{aryl}), 9.73 (s, 1H, OH), 10.68 (s, 1H, NH). ¹³C NMR spectrum, δ , ppm: 16.35, 55.86, 60.77, 91.86, 112.5, 114.1, 115.7, 121.9, 126.1, 126.7, 128.7, 128.9, 129.5, 135.2, 135.6, 147.5, 148.9, 155.1, 156.8, 163.1, 168.3, 169.5 (sp³, sp², sp carbons). Found, %: C, 64.36; H, 4.89; N, 10.29. Calculated, C₂₂H₂₀ClN₃O₃ (409.87) %: C, 64.47; H, 4.92; N, 10.25. Found, %: C, 61.09; H, 3.87; N, 11.47. Calculated, C₂₅H₁₉ClN₄O₅ (490.90) %: C, 61.17; H, 3.90; N, 11.41.

3.9 1-(2-(5-Amino-3-oxo-2,3-dihydro-1H-pyrazol-1-yl)-2-oxoethyl)-6-(4-chlorophenyl)-4-(4-hydroxy-3-methoxyphenyl)-2-oxo-1,2-dihydropyridine-3-carbonitrile (12)

A mixture of 2-(6-(4-chlorophenyl)-3-cyano-4-(4-hydroxy-3-methoxyphenyl)-2-oxopyridin-1(2H)-yl) acetohydrazide (**6**) (0.01 mole) and ethyl cyanoacetate (0.01 mole) with ethanol (20 mL) absolute was heated under reflux (6 hours). After cooling, the reaction mixture was diluted with water, and the formed precipitate was filtered off. Pale yellow solid (EtOH), mp = 180–182 °C, yield: 75%. IR spectrum, ν , cm⁻¹: 3321 (OH), 2223 (C≡N), 1692, 1652 (C=O). ¹H NMR spectrum, δ , ppm: 3.85 (bs, 2H, NH₂), 3.89 (s, 3H, OCH₃), 5.15 (s, NCH₂CO), 6.84 (s, 1H, H_{pyrazole}), 6.92–6.94 (m, 2H, H_{pyridine} and aryl), 6.96–6.99 (d, 1H, ³J = 8.0, Hz, H_{aryl}), 7.23–7.25 (d, 1H, ³J = 8.0, Hz, H_{aryl}), 7.57–7.59 (d, 2H, ³J = 8.40, Hz, H_{aryl}), 7.91–7.93 (d, 2H, ³J = 8.40, Hz, H_{aryl}), 9.70 (s, 1H, OH), 9.80 (s, 1H, NH). Found, %: C, 58.51; H, 3.73; N, 14.18, calculated, C₂₄H₁₈ClN₅O₅ (491.89) %: C, 58.60; H, 3.69; N, 14.24.

3.10 Biology

3.10.1 Cytotoxicity. Breast cancer (MCF-7), liver cancer (HepG2) cells, as well as normal (THLE2) cells were purchased from The National Cancer Institute, Cairo, Egypt. They were cultured in RPMI-1640 media with L-glutamine from Lonza Verviers SPRL in Belgium (cat#12-604F). The cells were then incubated in a NuAire chamber with a 5% CO₂ environment at 37 °C. In 96 wells, cells were seeded in triplicate at a density of 5

× 10⁴ cells. The chemicals were added to the cells on day two at doses of (0.01, 0.1, 1, 10, and 100 μM). Cell viability was determined using the MTT assay.^{50,51}

3.10.2 PIM-1 kinase inhibitory assay. Using the “HTScan® PIM-1 Kinase Assay Kit #7573,” compounds **5**, **9**, **10**, and staurosporine were tested for their ability to inhibit the PIM-1 kinase. They were dissolved in DMSO (0.1%), and five serial concentrations were prepared following Abdelaziz *et al.* 2018 (ref. 52) and the manufacturer's instructions.⁵³

3.10.3 Caspase 3, 8, 9 activity. Briefly, HepG2 (liver carcinoma) cells were cultured to a confluent monolayer and then treated with the tested samples at the IC₅₀ concentration as described earlier. After 48 h of treatment, the cells were harvested by trypsinization with 0.25% trypsin, followed by centrifugation for 5 min. The cell pellets were then washed twice with PBS for 20 min. Each is resuspended in a binding buffer. Apoptotic markers in both treated and untreated HepG2 cells were examined. The levels of caspase-3, caspase-8, and caspase-9 were assessed using ELISA colorimetric kits following the manufacturer's instructions. Specifically, the ELISA kits used were as follows: Human caspase-3 (Cat. No.: E-ELH0017) from Elabscience, Human caspase-8 (Cat. No.: E-EL-H0659) from Elabscience, Human caspase-9 (Cat. No.: E-EL-H0663) from Elabscience, and Human from Novus Biologicals USA.

3.10.4 Annexin V/PI staining flow cytometry. Overnight, HepG2 cells were added to 6-well culture plates at a density of 3–5 × 10³ cells per well and left to incubate. Compound **9** was applied to the cells at respective IC₅₀ values and left on for 48 hours. Afterwards, the cells and medium supernatants were washed with ice-cold PBS. Then, cells were suspended the cells in 100 μL of Annexin binding buffer solution “25 mM CaCl₂, 1.4 M NaCl, and 0.1 M Hepes/NaOH, pH 7.4” and incubated with “Annexin V-FITC solution (1 : 100) and propidium iodide (PI)” at a concentration equals 10 μg mL⁻¹ in the dark for 30 min. The flow cytometric data were analyzed using FlowJo version-10 software (TreeStar, Ashland, OR, USA).^{54–56}

3.10.5 Molecular docking. Using the protein data bank, the PIM-1 kinase protein structure (PDB = 2OBJ) was obtained, optimized by changing the amino acids, and then used Maestro to build, optimize, and energetically favor ligand configurations. Using AutoDock Vina software, a molecular docking investigation was conducted following routine work,⁵⁷ and lastly, docking associated with binding activities as measured by binding energies and interactions between receptors and ligands. The interaction analysis and binding disposition were examined using chimera.

4 Conclusion

Nicotinonitrile and pyrazolyl nicotinonitrile were synthesized, and their PIM-1 kinase inhibitors and caspase activators were investigated. A new Manich bases **6–8** were synthesized *via* reaction of pyridine **4** with piperidine, dimethyl amine, and morpholine in the presence of formalin. On the other hand, the pyrazolyl analogues **10–12** were synthesized *via* heterocyclization of acetohydrazide derivative **9** with acetylacetone,



malononitrile, and ethyl cyanoacetate, respectively, in ethanol. Compound **9** showed exceptional cytotoxic effects on MCF-7 and HepG2 cells among these derivatives, with IC₅₀ values of 0.34 μ M and 0.18 μ M, respectively. Curiously, compound **9** exhibited potent inhibition of PIM-1 kinase activity, with IC₅₀ values of 20.4 nM and 93.8% inhibition, respectively, compared to staurosporine, which had an IC₅₀ value of 16.7 nM and 95.6% inhibition. In addition, the molecular docking investigation showed that compound **9** bound to the PIM-1 kinase site similarly to a co-crystallized ligand, demonstrating a strong binding affinity.

Data availability

All data associated with this manuscript will be available upon reasonable request from the corresponding authors.

Author contributions

A. Hamza, A. Aboelmaged, H. A. Morsy synthesized the entire series of derivatives under the supervision of A. H. Moustafa, H. A. El-Sayed, S. M. El Rayes, and M.S. Nafie with the characterization of structure elucidation. At the same time, M. S. Nafie initiated the idea and design of the biology part by carrying out *in vitro* cytotoxic screening, enzyme targeting flow cytometry, and *in silico* studies with linguistic revision and manuscript finalizing. All authors contributed to data analysis and manuscript writing original drafts in their corresponding parts. All authors validated it in the final submitted form.

Conflicts of interest

The authors declare no conflict of interest.

References

- 1 R. L. Siegel, A. N. Giaquinto and A. Jemal, *Ca-Cancer J. Clin.*, 2024, **74**, 12–49.
- 2 M. Bachmann and T. Mörröy, *Int. J. Biochem. Cell Biol.*, 2005, **37**, 726–730.
- 3 X. Zhang, M. Song, J. K. Kundu, M.-H. Lee and Z.-Z. Liu, *J. Cancer Prev.*, 2018, **23**, 109–116.
- 4 X. Zhang, M. Song, J. K. Kundu, M.-H. Lee and Z.-Z. Liu, *J. Cancer Prev.*, 2018, **23**, 109.
- 5 L. S. Chen, S. Redkar, P. Taverna, J. E. Cortes and V. Gandhi, *Blood*, 2011, **118**, 693–702.
- 6 M. E. Abdelaziz, M. M. M. El-Miligy, S. M. Fahmy, M. A. Mahran and A. A. Hazzaa, *Bioorg. Chem.*, 2018, **80**, 674–692.
- 7 O. H. Rizk, M. Teleb, M. M. Abu-Serie and O. G. Shaaban, *Bioorg. Chem.*, 2019, **92**, 103189.
- 8 M. M. F. Ismail, A. M. Farrag, M. F. Harras, M. H. Ibrahim and A. B. M. Mehany, *Bioorg. Chem.*, 2020, **94**, 103481.
- 9 N. S. Magnuson, Z. Wang, G. Ding and R. Reeves, *Future Oncol.*, 2010, **6**, 1461–1478.
- 10 E. Kabir and M. Uzzaman, *Results Chem.*, 2022, **4**, 100606.
- 11 E. S. Tantawy, M. S. Nafie, H. A. Morsy, H. A. El-Sayed, A. H. Moustafa and S. M. Mohammed, *RSC Adv.*, 2024, **14**, 11098–11111.
- 12 N. Kerru, L. Gummidi, S. Maddila, K. K. Gangu and S. B. Jonnalagadda, *Molecules*, 2020, **25**, 1909.
- 13 A. Hamza, H. A. El-Sayed, A. H. Moustafa, S. M. El Rayes, A. Aboelmaged and R. A. Haggam, *J. Heterocycl. Chem.*, 2023, **60**, 803–813.
- 14 M. Alrooqi, S. Khan, F. A. Alhumaydhi, S. A. Asiri, M. Alshamrani, M. M. Mashraqi, A. Alzamami, A. M. Alshahrani and A. A. Aldahish, <http://www.eurekaselect.com>.
- 15 S. De, A. K. SK, S. K. Shah, S. Kazi, N. Sarkar, S. Banerjee and S. Dey, *RSC Adv.*, 2022, **12**, 15385.
- 16 H. A. El-Sayed, A. H. Moustafa, A. A. Fadda and K. E. Abd El-Rahman, *Russ. J. Gen. Chem.*, 2019, **89**, 339–347.
- 17 T. Tahir, M. Ashfaq, M. Saleem, M. Rafiq, M. I. Shahzad, K. Kotwica-Mojzych and M. Mojzych, *Molecules*, 2021, **26**, 4872.
- 18 M. M. M. El-Miligy, M. E. Abdelaziz, S. M. Fahmy, T. M. Ibrahim, M. M. Abu-Serie, M. A. Mahran and A. A. Hazzaa, *J. Enzyme Inhib. Med. Chem.*, 2023, **38**, 2152810.
- 19 A. M. Farrag, M. H. Ibrahim, A. B. M. Mehany and M. M. F. Ismail, *Bioorg. Chem.*, 2020, **105**, 104378.
- 20 N. Y. Megally Abdo, E. M. Samir and R. M. Mohareb, *J. Heterocycl. Chem.*, 2020, **57**, 1993–2009.
- 21 A. E. M. Mekky, S. M. H. Sanad, A. Y. Said and M. A. A. Elneairy, *Synth. Commun.*, 2020, **50**, 2376–2389.
- 22 R. M. Mohareb, F. M. Manhi, M. A. A. Mahmoud and A. Abdelwahab, *Med. Chem. Res.*, 2020, **29**, 1536–1551.
- 23 R. M. Mohareb, F. M. Manhi, M. A. A. Mahmoud and A. Abdelwahab, *Med. Chem. Res.*, 2020, **29**, 1536–1551.
- 24 I. W. Cheney, S. Yan, T. Appleby, H. Walker, T. Vo, N. Yao, R. Hamatake, Z. Hong and J. Z. Wu, *Bioorg. Med. Chem. Lett.*, 2007, **17**, 1679–1683.
- 25 Y. Zhang, C. Wu, N. Zhang, R. Fan, Y. Ye and J. Xu, *Int. J. Mol. Sci.*, 2023, **24**, 12724.
- 26 G. Li, Y. Cheng, C. Han, C. Song, N. Huang and Y. Du, *RSC Med. Chem.*, 2022, **13**, 1300–1321.
- 27 N. A. Warfel and A. S. Kraft, *Pharmacol. Ther.*, 2015, **151**, 41–49.
- 28 G. Roman, *Eur. J. Med. Chem.*, 2015, **89**, 743–816.
- 29 S. Murugappan, S. Dastari, K. Jungare, N. M. Barve and N. Shankaraiah, *J. Mol. Struct.*, 2024, **1307**, 138012.
- 30 H. A. El-Sayed, S. A. Said and A. M. Abd El-Hamid, *Synth. Commun.*, 2021, **51**, 3116–3124.
- 31 A. A. Mohamed, B. H. Asghar, A. H. Moustafa, H. A. El-Sayed, D. El-Sayed, A. S. A. Mohamed and K. A. Asla, *Russ. J. Gen. Chem.*, 2021, **91**, 2564–2580.
- 32 S. M. Mohammed, A. H. Moustafa, H. A. El-Sayed, A. Ayman and A. S. A. Mohamed, *Russ. J. Gen. Chem.*, 2021, **91**, S84–S88.
- 33 A. H. Moustafa, H. A. El-Sayed, A. E.-F. Z. Haikal and E. S. H. El Ashry, *Nucleos Nucleot. Nucleic Acids*, 2011, **30**, 340–352.
- 34 S. Chaudhuri, A. Ghosh and S. K. Chattopadhyay, *Green Synth. Approaches Biol. Relevant Heterocycl.*, 2021, 617–653.
- 35 P. W. Kenny, *J. Med. Chem.*, 2022, **65**, 14261–14275.



- 36 A. L. Hopkins, G. M. Keserü, P. D. Leeson, D. C. Rees and C. H. Reynolds, *Nat. Rev. Drug Discovery*, 2014, **13**, 105–121.
- 37 D. Hadži, J. Kidrič, J. Koller and J. Mavri, *J. Mol. Struct.*, 1990, **237**, 139–150.
- 38 P. D. Leeson and B. Springthorpe, *Nat. Rev. Drug Discovery*, 2007, **6**, 881–890.
- 39 S. Schultes, C. de Graaf, E. E. J. Haaksma, I. J. P. de Esch, R. Leurs and O. Krämer, *Drug Discov. Today Technol.*, 2010, **7**, e157–e162.
- 40 E. S. Tantawy, M. S. Nafie, H. A. Morsy, H. A. El-Sayed, A. H. Moustafa and S. M. Mohammed, *RSC Adv.*, 2024, **14**, 11098–11111.
- 41 F. G. Abdulrahman, R. Sabour, S. M. A. El-Gilil, A. B. M. Mehany and E. A. Taha, *J. Mol. Struct.*, 2024, **1295**, 136811.
- 42 R. M. Mohareb, N. Y. M. Abdo and W. W. Wardakhan, *Med. Chem. Res.*, 2017, **26**, 2520–2537.
- 43 M. S. Nafie, A. M. Amer, A. K. Mohamed and E. S. Tantawy, *Bioorg. Med. Chem.*, 2020, **28**, 115828.
- 44 S. Mohamady, A. F. Khalil, B. H. Naguib, M. S. Nafie, H. O. Tawfik and M. A. Shaldam, *Bioorg. Chem.*, 2024, **143**, 106988.
- 45 Y. Shi, *Mol. Cell*, 2002, **9**, 459–470.
- 46 S. E. Logue and S. J. Martin, *Biochem. Soc. Trans.*, 2008, **36**, 1–9.
- 47 S. Kumar, *Cell Death Differ.*, 1999, **6**, 1060–1066.
- 48 I. Budihardjo, H. Oliver, M. Lutter, X. Luo and X. Wang, *Annu. Rev. Cell Dev. Biol.*, 1999, **15**, 269–290.
- 49 E. S. Tantawy, M. S. Nafie, H. A. Morsy, H. A. El-Sayed, A. H. Moustafa and S. M. Mohammed, *RSC Adv.*, 2024, **14**, 11098–11111.
- 50 T. Mosmann, *J. Immunol. Methods*, 1983, **65**, 55–63.
- 51 E. S. Tantawy, A. M. Amer, E. K. Mohamed, M. M. Abd Alla and M. S. Nafie, *J. Mol. Struct.*, 2020, **1210**, 128013.
- 52 M. E. Abdelaziz, M. M. M. El-Miligy, S. M. Fahmy, M. A. Mahran and A. A. Hazzaa, *Bioorg. Chem.*, 2018, **80**, 674–692.
- 53 CST, HTScan® Pim-1 Kinase Assay Kit, www.cellsignal.com/products/cellular-assay-kits/htscan-pim-1-kinase-assay-kit/7573, accessed July 17, 2020.
- 54 M. S. Nafie, K. Arafa, N. K. Sedky, A. A. Alakhdar and R. K. Arafa, *Chem. Biol. Interact.*, 2020, **324**, 109087.
- 55 M. S. Nafie, A. M. Amer, A. K. Mohamed and E. S. Tantawy, *Bioorg. Med. Chem.*, 2020, **28**, 115828.
- 56 E. M. Gad, M. S. Nafie, E. H. Eltamany, M. S. A. G. Hammad, A. Barakat and A. T. A. Boraie, *Molecules*, 2020, **25**, 2523.
- 57 M. S. Nafie, M. A. Tantawy and G. A. Elmgeed, *Steroids*, 2019, **152**, 108485.

